

Mn(II) Complex of Lipophilic Group-Modified Ethylenediaminetetraacetic Acid (EDTA) as a New Hepatobiliary MRI Contrast Agent

Keyu Chen, Pan Li, Chunrong Zhu, Zhiyang Xia, Qian Xia, Lei Zhong, Bin Xiao, Tao Cheng, Changqiang Wu, Chengyi Shen, Xiaoming Zhang,* and Jiang Zhu*

Cite This: *J. Med. Chem.* 2021, 64, 9182–9192

Read Online

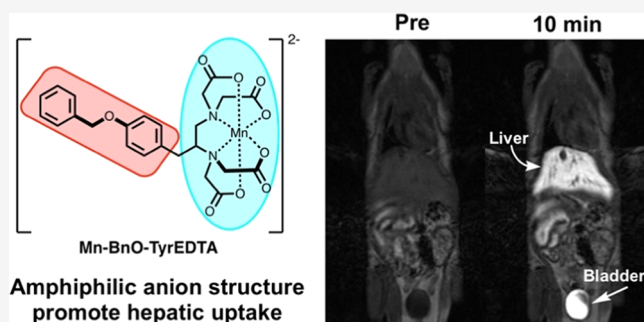
ACCESS |

Metrics & More

Article Recommendations

Supporting Information

ABSTRACT: Liver-specific contrast agents (CAs) can improve the Magnetic resonance imaging (MRI) detection of focal and diffuse liver lesions by increasing the lesion-to-liver contrast. A novel Mn(II) complex, Mn-BnO-TyrEDTA, with a lipophilic group-modified ethylenediaminetetraacetic acid (EDTA) structure as a ligand to regulate its behavior in vivo, is superior to Gd-EOB-DTPA in terms of a liver-specific MRI contrast agent. An MRI study on mice demonstrated that Mn-BnO-TyrEDTA can be rapidly taken up by hepatocytes with a combination of hepatobiliary and renal clearance pathways. Bromosulfophthalein (BSP) inhibition imaging, biodistribution, and cellular uptake studies confirmed that the mechanism of hepatic targeting of Mn-BnO-TyrEDTA is the hepatic uptake of the amphiphilic anion contrast agent mediated by organic anion transporting polypeptides (OATPs) expressed by functional hepatocytes.



INTRODUCTION

Magnetic resonance imaging (MRI) is one of the most powerful noninvasive diagnostic tools in medical imaging and biomedical research. Without using ionizing radiation, this technique can generate superb tissue contrast imaging with high spatial resolution.¹ Due to its relatively low sensitivity, more than one-third of clinical MR scans are being contrast-enhanced by the use of MRI contrast agents (CAs), which can catalytically shorten the relaxation times (T_1 and T_2) of bulk water protons to increase signal intensity. Compared with unenhanced MR images, contrast-enhanced MRI can produce more morphologic and functional information, which results in more accurate diagnosis of diseases. The most widely used MR CAs are dominated by the paramagnetic chelates of gadolinium-based contrast agents (GBCAs), owing to gadolinium(III)'s high effective magnetic moment and relatively slow electronic spin relaxation.²

To reduce the toxicity of free Gd^{3+} ion, the gadolinium ion is chelated with multidentate ligands (chelators), either macrocyclic (H4DOTA) or linear (HS-DTPA), to form high stability (thermodynamic and kinetic) charged or charge-neutral chelates (Chart 1). It is well known that the chemical structure of ligand determined the overall biology behavior of these Gd^{3+} chelates in vivo (biodistribution, pharmacokinetics, pharmacodynamics, and safety profiles).^{3–5} In general, most clinically approved small molecular gadolinium chelates are called nonspecific, extracellular fluid (ECF) agents, as they are highly

hydrophilic, do not bind to proteins or receptors, and are rapidly excreted unmetabolized in urine.^{2,6–8}

Usually, an amphiphilic structure formed by introducing lipophilic groups (e.g., aromatic or steroid structures) to the ligand of a highly hydrophilic gadolinium chelate will promote hepatic uptake. For instance, Gd-EOB-DTPA and Gd-BOPTA, two Gd-DTPA-derived chelates that are composed of an ethoxybenzyl moiety and a benzoylmethyl moiety, respectively, are the most widely used contrast agents in clinic hepatic MR imaging. Liver-specific CA-enhanced liver MRI can provide valuable anatomic and functional diagnosis information in numerous focal and diffuse liver lesions,⁹ such as facilitating the differentiation of focal nodular hyperplasia (FNH) from hepatocellular carcinoma (HCA),^{10,11} quantitatively assessing regarding liver perfusion and hepatocyte function.

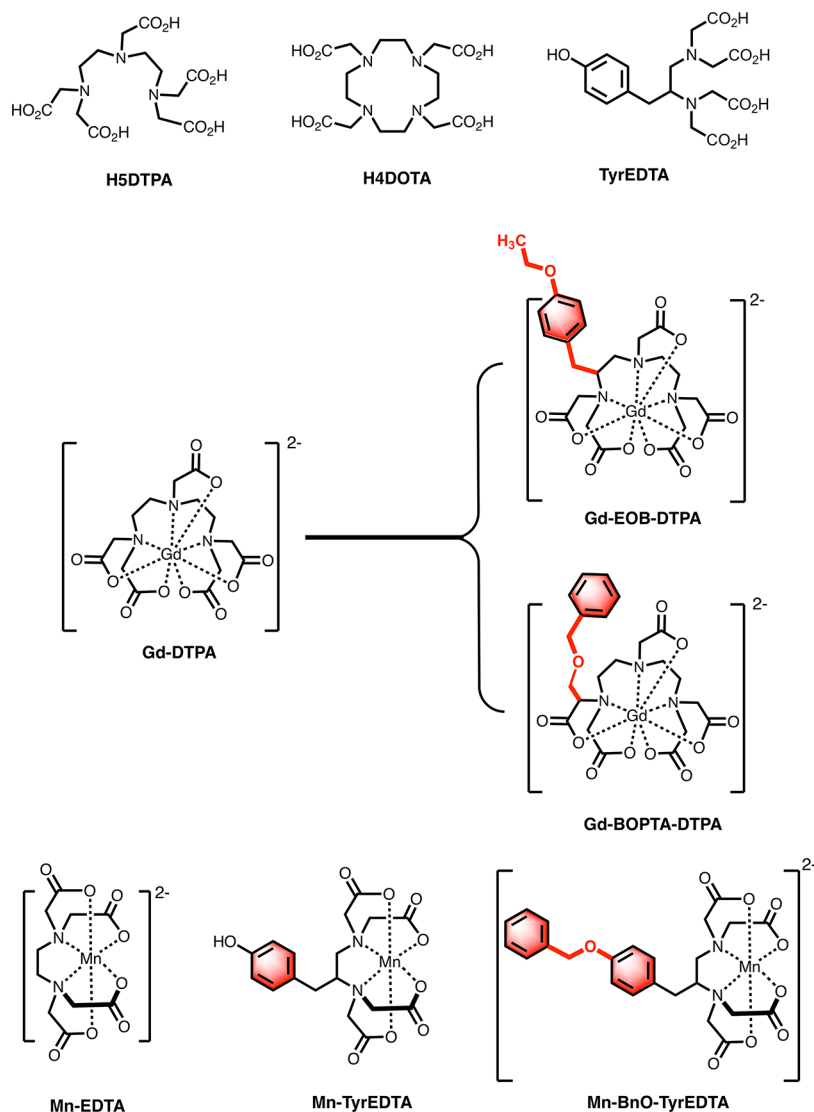
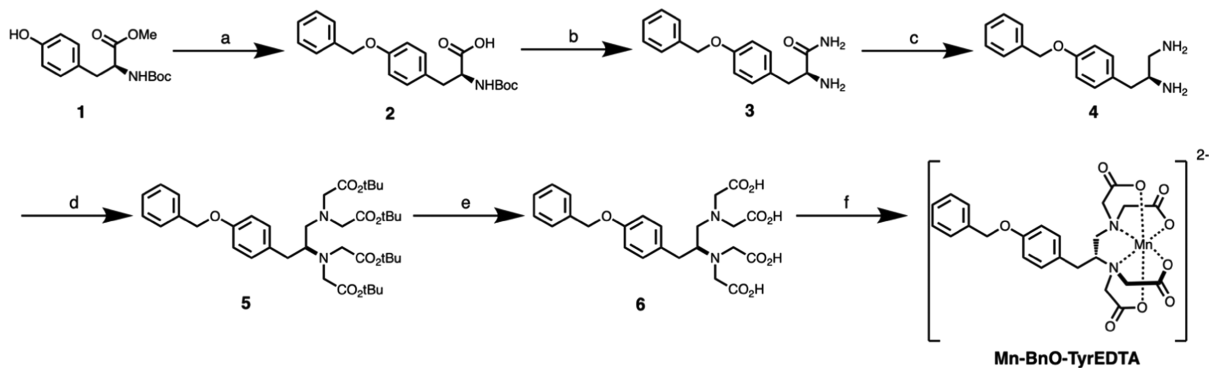
Recent studies revealed that highly expressed organic anion transporting polypeptides (OATPs; OATP1B1 and OATP1B3) on hepatocyte membranes are the main transporters of amphiphilic structural small-molecule liver-specific

Received: March 5, 2021

Published: June 21, 2021



Chart 1. Ligand and Chelate Structures Discussed in This Paper

Scheme 1. Synthesis Procedure of the Mn-BnO-TyrEDTA Complex^a

^aReagents and conditions. a. (i) K_2CO_3 , KI, BnCl, 90°C , 6.0 h; (ii) NaOH, H_2O , THF, 50°C , 1.0 h, and then acidified with diluted HCl; b. (i) isobutyl chloroformate, DIPEA, THF, rt, 1.0 h, and then $\text{NH}_3(\text{g})$, 24.0 h, rt; (ii) TFA, CH_2Cl_2 , rt, 12.0 h; c. $\text{BH}_3\cdot\text{THF}$, THF, refluxed, 24.0 h; d. *tert*-butyl bromoacetate, DIPEA, KI, acetonitrile (ACN), 50°C , 12.0 h; e. TFA, dichloromethane (DCM), 12.0 h; and f. $\text{MnCl}_2\cdot 4\text{H}_2\text{O}$, NaOH (1.0 M), pH 7.4.

contrast agents (e.g., Gd-EOB-DTPA).^{12–16} High-spin manganese(II) (5/2) with five unpaired electrons and relatively slow electron relaxation has lower intrinsic toxicity

and a faster water-exchange rate than gadolinium(III). Recently, the identification of nephrogenic systemic fibrosis (NSF)^{17–20} and brain gadolinium deposition,^{21–24} a rare but

Table 1. r_1 and r_2 in pH 7.4 Tris Buffer and 4.5% w/v Bovine Serum Albumin at 0.47 T and 32 °C

chelate	r_1 pH 7.4 tris ($\text{mM}^{-1} \text{s}^{-1}$)	r_2 pH 7.4 tris ($\text{mM}^{-1} \text{s}^{-1}$)	r_1 BSA ($\text{mM}^{-1} \text{s}^{-1}$)	r_2 BSA ($\text{mM}^{-1} \text{s}^{-1}$)
Mn-EDTA	2.83 ± 0.06	3.90 ± 0.06	3.46 ± 0.07	4.57 ± 0.06
Mn-BnO-TyrEDTA	4.34 ± 0.08	6.21 ± 0.17	15.81 ± 1.72	20.70 ± 2.36
Gd-EOB-DTPA	6.15 ± 0.11	6.99 ± 0.12	8.36 ± 0.23	9.41 ± 0.38

serious disorder associated with adventurous Gd(III), has led to manganese(II) as an attractive alternative to gadolinium(III) for MRI application. For example, excellent kinetically inert Mn-based MR CAs such as Mn-PyC3A,²⁵ Mn-bispidine chelate,²⁶ and liver-specific Mn(II) CAs have been reported.²⁷

It is well known that the structure of ethylenediaminetetraacetic acid (EDTA) and its derivatives have been widely used as ligands for chelating Mn^{2+} in the research of manganese-based contrast agents.^{28,29} Previously, we reported a hexameric Mn(II) dendrimer that was synthesized from a tyrosine-derived bifunctional precursor featuring a backbone-substituted EDTA structure (named TyrEDTA)³⁰ (Chart 1, Mn-TyrEDTA). The corresponding moderate molecular weight Mn(II) dendrimer exhibited high relaxivity at different fields and mixed renal and hepatobiliary clearance in vivo.³¹ In this work, we are pursuing the further development of this bifunctional structure to develop a new T_1 liver-specific Mn^{2+} contrast agent ($[\text{Mn}(\text{TyrEDTA})]^{2-}$) by introducing a lipophilic group on the TyrEDTA ligand (BnO-TyrEDTA; Chart 1). The synthesis, characterization, and MRI liver enhancement patterns of this new amphiphilic, anionic Mn(II) complex in mice were demonstrated. In addition, the hepatic uptake mechanism was further investigated by OATP inhibition imaging and cell uptake study.

RESULTS AND DISCUSSION

Synthesis and Characterization. The ligand (BnO-TyrEDTA, compound 6) was synthesized via a multiple-step reaction with Boc-L-tyrosine methyl ester (compound 1) as the starting material (Scheme 1). In brief, the phenol group of compound 1 was protected by the benzyl group and then the methyl ester group was hydrolyzed to give compound 2. The acid group of compound 2 was activated with isobutyl chloroformate and treated with ammonia gas, and then the Boc group was removed to give compound 3. The amide carbonyl of compound 3 was reduced by the borane–tetrahydrofuran (THF) complex to afford the key intermediate diamine (compound 4). Exhaustive N-alkylation of compound 4 with *tert*-butyl bromoacetate and then acid cleavage of the *tert*-butyl ester yielded the ligand compound (compound 6). To ensure the preparation of the Mn(II) complex of 1:1 Mn/ligand, the precise ligand concentration was determined by titration of an aliquot ligand solution with Mn(II).³¹ Finally, the corresponding Mn(II) complex (abbreviated as Mn-BnO-TyrEDTA) was prepared by mixing the ligand and $\text{MnCl}_2 \cdot 4\text{H}_2\text{O}$ at pH 7.4 proportionally based on the titration data (Figure S24 in the Supporting Information). All of the intermediate compounds and the final product were characterized by spectroscopic techniques, such as NMR and mass spectrometry (Figures S1–S22 in the Supporting Information).

Relaxivity. The efficiency of a contrast agent is expressed by its relaxivity (r_1 or r_2 , in $\text{mM}^{-1} \text{s}^{-1}$), which is defined as the change of the relaxation rate ($R_{1,2} = 1/T_{1,2}$ in units of s^{-1}) of the water protons upon addition of a normalized concentration of the contrast agent (in units of mmol/L , mM).³² We

measured the relaxivities (r_1 and r_2) of Mn-EDTA, Mn-BnO-TyrEDTA, and Gd-EOB-DTPA (Table 1). At 0.47 T, the r_1 value of Mn-BnO-TyrEDTA was $4.34 \text{ mM}^{-1} \text{ s}^{-1}$ (in Tris buffer (50 mM), pH = 7.4) and increased to $15.81 \text{ mM}^{-1} \text{ s}^{-1}$ (in bovine serum albumin (BSA), 4.5%), higher than those of Gd-EOB-DTPA and Mn-EDTA (8.36 and $3.46 \text{ mM}^{-1} \text{ s}^{-1}$ in BSA). The lipophilic group in Mn-BnO-TyrEDTA promotes its strong binding to albumin, as evidenced by the significant increase of relaxivity in the BSA solution since the tumbling rate slows down after macromolecule complex formation.

log P. Due to the negatively charged exterior of the cell, most anionic GBCAs are usually not internalized by the cells and considered as extracellular fluid (ECF) agents. Liver-specific contrast agents such as Gd-EOB-DTPA could be structurally considered as amphiphilic derivatives of highly polar hydrophilic anionic Gd-DTPA covalently linked to a lipophilic *p*-ethoxybenzyl (EOB) moiety. Caravan et al. found that the liver uptake and the rate of blood clearance are directly correlated with log *P* values through the study of the structure–activity relationship (SAR) of a series of small molecular Mn(II) complexes.²⁷ In our work, we measured the estimated log *P* values of Mn-BnO-TyrEDTA and Mn-EDTA using the reverse-phase high-performance liquid chromatography (HPLC) method. Mn-BnO-TyrEDTA (log *P* = 0.18) shows higher lipophilicity than Mn-EDTA (log *P* = −2.27) based on the estimated log *P* values (Table S1 in the Supporting Information).

Cell Viability Assay. The toxicity of Mn-BnO-TyrEDTA was evaluated by the cell viability assay with commercially available Gd-EOB-DTPA as a comparison (Figure 1). Raw

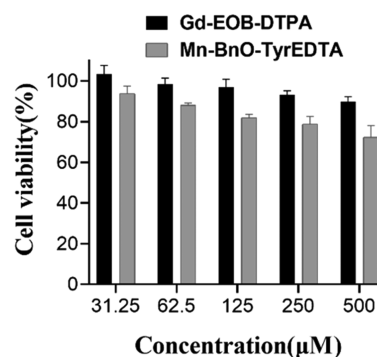


Figure 1. Cell cytotoxicity assay via CCK-8 against RAW 264.7 cells with different concentrations of Mn-BnO-TyrEDTA and Gd-EOB-DTPA at 37 °C for 24 h. Error bars represent the standard deviation (\pm SD) on a triplicate analysis.

264.7 cells were incubated with different concentrations of CAs for 24 h at 37 °C, and the cytotoxicity was estimated using the Cell Counting Kit-8. At low drug loading concentrations ($<125 \mu\text{M}$), it was found that Mn-BnO-TyrEDTA did not show appreciable cytotoxicity, and cells were significantly viable with viability over 80% after incubation for 24 h. At high concentrations ($>250 \mu\text{M}$), the cytotoxicity of Mn-BnO-TyrEDTA was higher and the cell viability percentage dropped

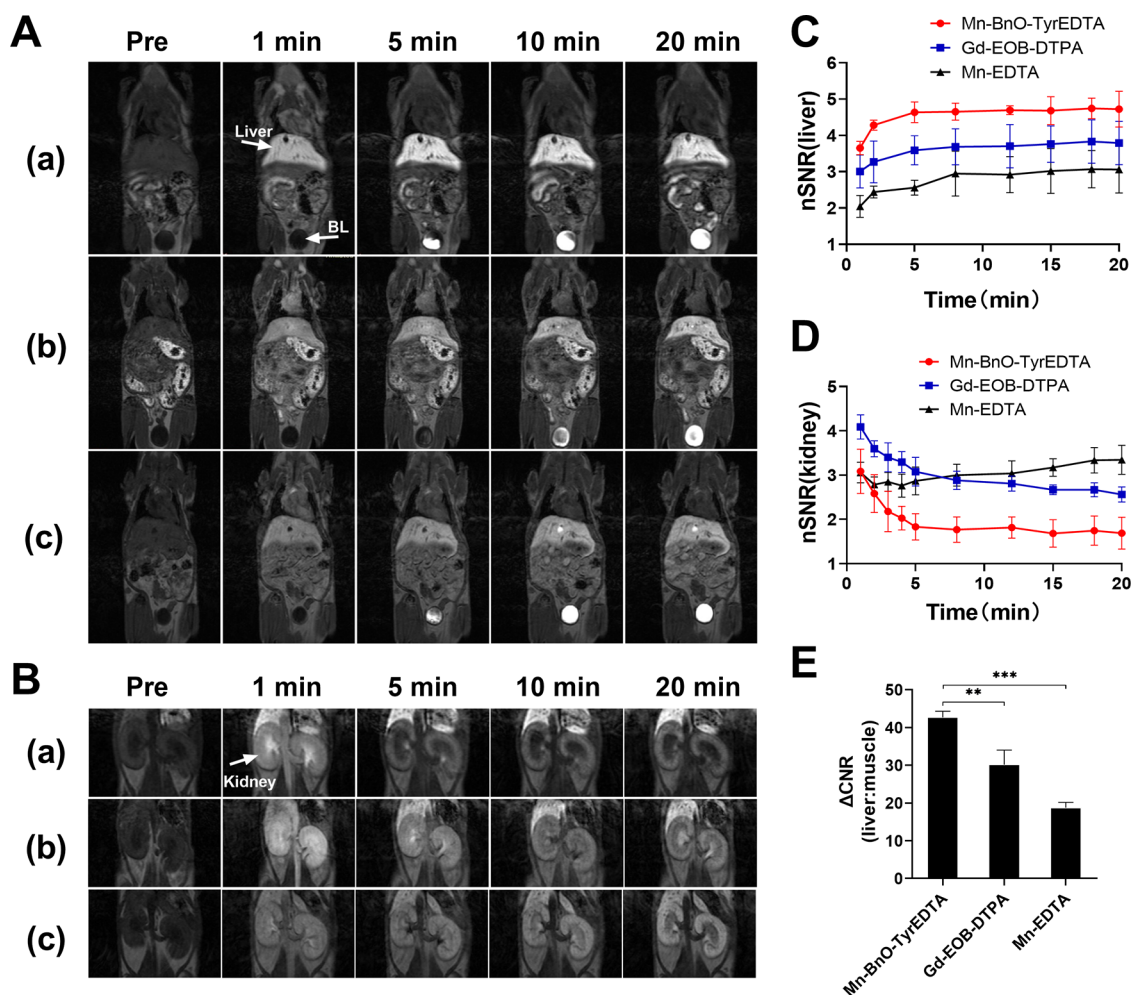


Figure 2. Spoiled gradient recalled echo T1-weighted images (SPGR-T1WI) of normal Swiss mice recorded at 3.0 T capturing the liver (A) and kidneys (B) obtained prior, 1, 5, 10, and 20 min after tail vein injection of Mn-BnO-TyrEDTA (a), Gd-EOB-DTPA (b), and Mn-EDTA (c) at a dose of 0.1 mmol/kg, respectively. BL, bladder. Graphs show the normalized signal-to-noise ratio (nSNR) time course in the liver (C) and kidneys (D) after injection of CAs. (E) Δ CNR (liver vs muscle) recorded 5 min postinjection demonstrates that the liver enhancement is the greatest for Mn-BnO-TyrEDTA. Data are reported as mean \pm standard deviation ($n = 3$; $**P < 0.01$ and $***P < 0.001$).

to 75% (500 μ M, 90% for Gd-EOB-DTPA). It is noteworthy that the cytotoxicity could be negligible, as found from the rapid clearance of Mn-BnO-TyrEDTA in the pharmacokinetic study on rats.

In Vivo MR Images of Mice. Gd-EOB-DTPA-enhanced MRI is now the gold standard for the diagnosis of liver-specific diseases³³ with approximately 50% of the administered dose being taken up into hepatocytes and excreted via the biliary system.^{34,35} To investigate the hepatobiliary imaging capacity and pharmacokinetics of Mn-BnO-TyrEDTA, we performed dynamic contrast-enhanced (DCE) MRI studies in normal mice at 3.0 T using a clinical whole-body scanner with Gd-EOB-DTPA and Mn-EDTA as comparisons. After the tail was intravenously administrated with the same dose of contrast agents, mice were scanned starting from preinjection to 20 min postinjection using a spoiled gradient recalled echo T1-weighted image (SPGR-T1WI) sequence.

Figure 2A,B showed the coronal T1-weighted images recorded at baseline, 1, 5, 10, and 20 min postinjection. The signal intensity of the liver and kidneys were measured, and the normalized signal-to-noise ratio (nSNR) was calculated as a function of time to analyze the contrast enhancement behavior in vivo of three contrast agents (Figure 2C,D). Both Mn-BnO-

TyrEDTA and Gd-EOB-DTPA produced a significantly greater and more prolonged liver signal enhancement than Mn-EDTA, especially between 5 and 20 min at the same dose (Figure 2A). Among the three complexes, Mn-BnO-TyrEDTA produced the overwhelmingly highest signal-to-noise ratio (SNR) in the liver within 20 min postinjection (Figure 2C) and the strongest liver-to-muscle contrast-to-noise ratio (Δ CNR) at 5 min postinjection (Figure 2E). The relaxivity in the liver tissue was increased probably due to the increased microviscosity inside the hepatocyte or the transient interaction with intracellular proteins.³⁶

All three CAs showed renal excretion revealed by the images of the kidneys and bladder with the initial strong kidney enhancement at 1 min and the subsequent enhancement of the urinary bladder between 5 and 20 min (Figure 2B). The renal excretion of Mn-EDTA was much slower than those of Mn-BnO-TyrEDTA and Gd-EOB-DTPA evidenced by an increase in the kidney signal after 8 min (Figure 2D). The structure of Mn-EDTA is kinetically less inert than Mn-BnO-TyrEDTA, which was the backbone-substituted structure of EDTA. Both slow renal excretion and liver enhancement of Mn-EDTA could be attributed to the free Mn^{2+} ion dissociated from Mn-EDTA. Overall, Mn-BnO-TyrEDTA with an amphiphilic and

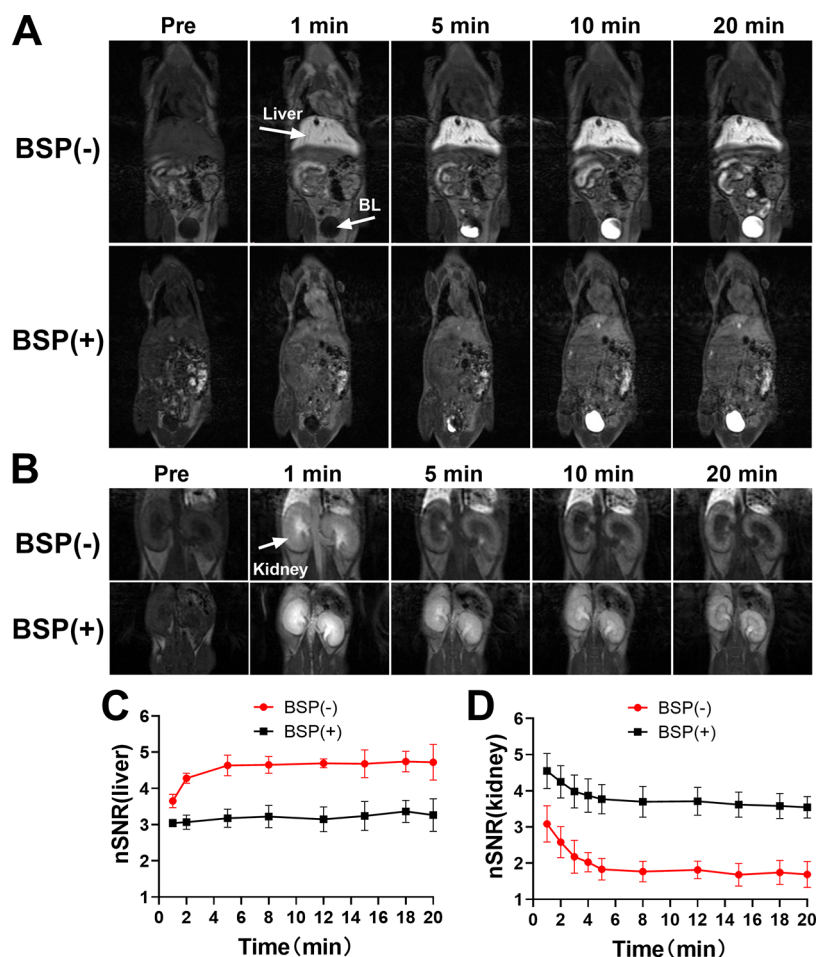


Figure 3. In vivo spoiled gradient recalled echo T1-weighted imaging (SPGR-T1WI) capturing the liver (A) and kidneys (B) after injection of Mn-BnO-TyrEDTA (0.1 mmol/kg) in the absence and presence of bromosulphthalein (BSP). Normalized SNR (nSNR) time courses in the liver (C) and kidneys (D) that were recorded out to 20 min from the MR images. BL, bladder. Data are reported as mean \pm SD ($n = 3$).

negatively charged structure shows excellent liver-specific contrast enhancement and a combination of hepatobiliary and renal clearance in our imaging study in vivo.

Bromosulphthalein (BSP) Inhibition Images of Mice. Organic anion transporting polypeptides (OATPs) are the key transporters for the disposition of various drugs and endogenous substrates, influencing the pharmacokinetics of multiple classes of drugs and participating in many clinical drug–drug interactions.³⁷ The hepatic uptake of Gd-EODTPA is also mediated by OATPs (OATP1B1 and OATP1B3) and known to be inhibited by bromosulphthalein (BSP)³⁸ and rifampicin.³⁹

We performed the DCE-MR study to explore the liver-targeting mechanism of Mn-BnO-TyrEDTA using BSP as a competitive inhibitor. BSP was administered intravenously with a blood concentration of 0.1 mM maintained before bolus injection of Mn-BnO-TyrEDTA. Compared with the BSP (-) group, the BSP (+) group had less pronounced liver enhancement and maintained lower signal intensity (nSNR) during the experiment (Figure 3). In contrast, the BSP (+) group showed better renal enhancement and remained stable until 20 min. The pronounced decrease in hepatic enhancement after the preadministration of BSP can be explained by the competitive inhibition of the hepatocellular uptake of Mn-BnO-TyrEDTA. As a surrogate, the decrease of hepatic excretion results in the enhanced renal clearance of the

contrast agent. The mechanism of liver-targeting of Mn-BnO-TyrEDTA can be attributed to the hepatic uptake mediated by OATPs expressed by hepatocytes based on the above BSP inhibition imaging study.

Cell Uptake Study. We further performed the cell uptake study to verify that OATPs (OATP1B1 and OATP1B3) are master transporters in the hepatic uptake of Mn-BnO-TyrEDTA based on the results of BSP inhibition imaging. Herein, we performed the cell uptake study for Mn-BnO-TyrEDTA in the OATP1B1-transfected HEK-293 cell line (HEK-OATP1B1). Both real-time quantitative polymerase chain reaction (PCR) analysis and immunofluorescence staining indicated high expression of OATP1B1 in HEK-OATP1B1 cells. It should be noted that low expression of OATP1B1 in HEK-293 cells could be observed in the immunofluorescence assay (Figure S27 in the Supporting Information). As illustrated in Figure 4A, the uptake rate of Mn-BnO-TyrEDTA by HEK-OATP1B1 cells was significantly higher than HEK-293 cells (approximately 2-fold higher after incubation for 30 min with 0.1 mM drug loading). Competitive inhibition studies using BSP as an inhibitor of OATP1B1 could inhibit nearly 50% of the hepatic uptake of Mn-BnO-TyrEDTA, further confirming the importance of OATP1B1 in the hepatic uptake of the contrast agent (Figure 4B).

Biodistribution and Biliary Excretion. The in vivo biodistribution in nine tissues (heart, brain, liver, spleen, lungs,

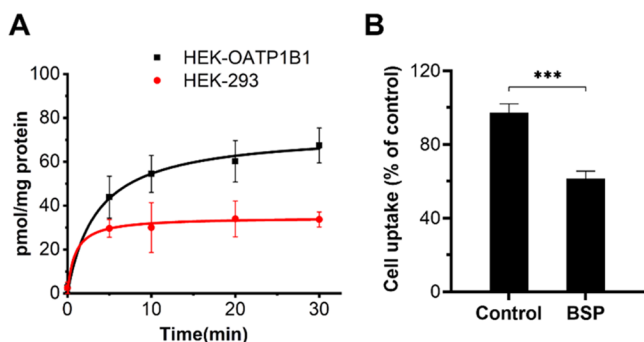


Figure 4. (A) Uptake of Mn-BnO-TyrEDTA (0.1 mM) in HEK cells transfected with human OATP1B1 (HEK-OATP1B1) and normal control cells (HEK-293) after incubation for 5–30 min. (B) Uptake of Mn-BnO-TyrEDTA (100 μ M) in HEK-OATP1B1 cells was measured at 10 min in the absence (control) and presence of BSP (100 μ M). Mean \pm SD is given for $n = 3$ experiments. *** $P < 0.001$.

kidneys, bone, muscle, and small intestine) of the Mn content was quantitatively measured by inductively coupled plasma mass spectrometry (ICP-MS). The bile was collected (up to about 80 min postinjection) and the Mn content was quantified to evaluate the biliary excretion of Mn-BnO-TyrEDTA. The ICP-MS data show that about 44 and 7% of the accumulated administered dose was in the liver at 5 min and 30 min, respectively (Figure 5A). The change of the accumulated dose in the liver at the two different time points (5 vs 30 min) was roughly in agreement with the dose recovered in the bile over this period (5–30 min). During this period, a rapid washout of the contrast agent in the liver could be estimated (approximately 37%), which was roughly consistent with the biliary excretion of the contrast agent (approximately 25%; Figure 5B). Biliary clearance data indicate that approximately 50% of the administered dose is excreted within 80 min.

In addition to the liver, the kidneys showed relatively high Mn accumulation, resulting from glomerular excretion via the renal pathway and Mn levels returned to the baseline within 24 h. Therefore, the *in vivo* biodistribution data strongly suggest that Mn-BnO-TyrEDTA is excreted by both renal and hepatobiliary routes. This dual excretion pattern of Mn-BnO-TyrEDTA is very similar to the excretion pattern of liver-specific Gd-EOB-DTPA.

Pharmacokinetic Study. To study the pharmacokinetic behavior of Mn-BnO-TyrEDTA, the manganese content in

plasma at different time points was quantitatively analyzed by ICP-MS after single-dose intravenous injection (0.1 mmol/kg; Figure 6). Table 2 shows the pharmacokinetic parameters

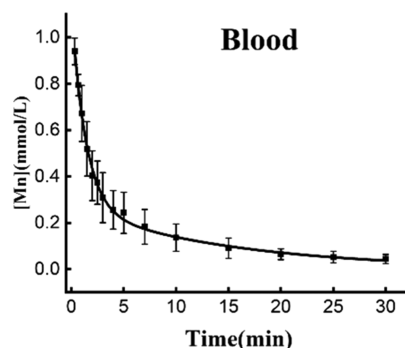


Figure 6. Plasma Mn content–time curve of Mn-BnO-TyrEDTA in rats ($n = 6$). Data are reported as mean \pm SD.

Table 2. Pharmacokinetic Parameters of Mn-BnO-TyrEDTA^a

parameter	[Mn]-time	unit
$t_{1/2\alpha}$	0.83 ± 0.24	min
$t_{1/2\beta}$	9.33 ± 1.92	min
AUC_{0-t}	5.28 ± 1.50	mmol/L·min
V_d	0.078 ± 0.013	(mmol/kg)/(mmol/L)
CL	0.019 ± 0.006	L/kg/min

^a $t_{1/2\alpha}$ and $t_{1/2\beta}$ indicate distribution and elimination half-lives, respectively. AUC_{0-t} indicates the area under the drug–time curve from the start of the administration to the last observation time point. V_d , apparent volume of distribution; CL, clearance rate.

estimated from the Mn-BnO-TyrEDTA plasma clearance data. Mn-BnO-TyrEDTA exhibits rapid biexponential plasma clearance, which is the typical behavior of extracellular contrast agents, with a half-life of distribution ($t_{1/2\alpha}$) of 0.83 ± 0.24 min and a half-life of elimination ($t_{1/2\beta}$) of 9.33 ± 1.92 min.

CONCLUSIONS

In summary, we have designed, synthesized, and characterized a novel Mn(II) complex with a lipophilic group-modified EDTA structure as a ligand and investigated its diagnostic ability as a hepatobiliary specific MRI contrast agent. The *in vivo* MRI study on mice demonstrated that this Mn(II)

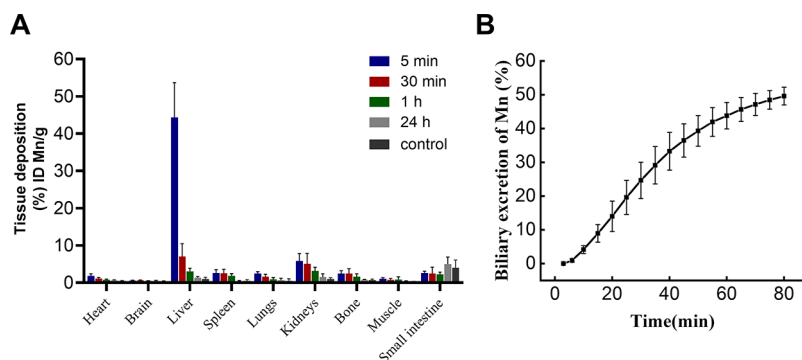


Figure 5. (A) Biodistribution study of Mn-BnO-TyrEDTA (0.1 mmol/kg) in normal mice represented by the Mn percentage in each tissue ($n = 6$). (B) Biliary excretion of Mn-BnO-TyrEDTA in rats after intravenous (IV) administration of Mn-BnO-TyrEDTA at 0.1 mmol/kg ($n = 6$). Data are reported as mean \pm SD.

complex, Mn-BnO-TyrEDTA, can produce superb liver enhancement with a combination of hepatobiliary and renal clearance pathways, which is similar to that of the clinically used liver-specific agent Gd-EOB-DTPA. In vivo biodistribution further confirmed its hepatic specificity, and plasma pharmacokinetic studies revealed its rapid plasma distribution and elimination rate, which is typical for extracellular fluid contrast agents. Finally, BSP inhibition imaging and cellular uptake studies confirmed that the mechanism of hepatic targeting of Mn-BnO-TyrEDTA is the hepatic uptake of the amphiphilic anion contrast agent mediated by OATPs expressed by functional hepatocytes. Mn-BnO-TyrEDTA, which showed excellent liver specificity with an OATP-transport mechanism in our study, may contribute to the MRI diagnosis of cancer with altered OATP expression (e.g., liver, breast, and prostate cancer).⁴⁰

EXPERIMENTAL SECTION

General Remarks. All reagents were purchased from Aladdin Industrial Corporation (Shanghai, China), such as Boc-tyr-OMe/THF/TFA/N, *N*,*N*-diisopropylethylamine/isobutyl chloroformate/*tert*-butyl bromoacetate, etc., $\text{MnCl}_2 \cdot 4\text{H}_2\text{O}$ was purchased from Sigma-Aldrich (St. Louis, MO), and anhydrous acetonitrile/benzyl bromoacetate was purchased from Alfa-Aesar (Ward Hill, MA). Other common reagents are domestic analytical pure (methanol, ethanol, petroleum ether, acetonitrile, dichloromethane, concentrated hydrochloric acid, dichloro-sulfoxide, sodium bicarbonate, sodium chloride, anhydrous sodium sulfate, etc.). All reagents were purchased commercially and used without further purification. The purity of all compounds by biological evaluation was $\geq 95\%$. Purity was evaluated by ^1H NMR and the purity of the final complex compound was evaluated by HPLC using the method described in HPLC for estimating log *P*. Ultrapure water (UP) was used for all experimental procedures. Mass (electrospray ionization mass spectrometry (ESI-MS)) spectra and nuclear magnetic resonance (^1H NMR 400 MHz, Bruker Advance) hydrogen spectra were commonly used to identify the structures. Tetramethyl silane (TMS) was used as an interior standard for chemical shifts. No unexpected or unusual high safety hazards were encountered during experimental procedures.

All experiments were executed in accordance with the Guidelines for Care and Use of Laboratory Animals and were approved by the Ethics Committee of North Sichuan Medical College. All animals were fasted 12 h prior to drug administration and had access to water ad libitum and were fed 4 h postdose.

Synthesis and Characterization. *3-(4-Benzyloxy-phenyl)-2-tert-butoxycarbonylamino-propionic Acid (2)*. (i) Compound 1 (20 g, 67.72 mmol), K_2CO_3 (20.59 g, 148.59 mmol), and KI (1.12 g, 6.77 mmol) were dissolved in ACN (120 mL), and Bn-Cl (9.43 g, 74.49 mmol) was slowly added and the mixture was stirred for 6 h in a 90 °C oil bath. The reaction was monitored and confirmed by thin-layer chromatography (TLC). Inorganic salts were removed using a filter and the filtrate was rotated to evaporate the solvent. The crude compound was recrystallized with ethanol, and the pure product was collected as a white solid. Yield: 25.0 g (96%). ^1H NMR (400 MHz, DMSO) δ 7.46–7.26 (m, 5H), 7.14 (d, *J* = 8.0 Hz, 2H), 6.92 (d, *J* = 8.0 Hz, 2H), 5.06 (s, 2H), 4.19–3.98 (m, 1H), 3.59 (s, 3H), 2.99–2.68 (m, 2H), 1.29 (s, 9H). ^{13}C NMR (100 MHz, DMSO) δ 173.18, 157.47, 155.90, 137.61, 130.57, 130.08, 128.88, 128.24, 128.09, 114.96, 78.78, 69.55, 55.92, 52.22, 36.05, 28.56. (*m/z*) for $\text{C}_{22}\text{H}_{27}\text{NO}_5$: calcd, 408.18 [M + Na]⁺, 384.18 [M – H][–]; found, 408.1 [M + Na]⁺, 384.2 [M – H][–].

(ii) *3-(4-Benzyloxy-phenyl)-2-tert-butoxycarbonylamino-propionic acid* (25 g, 67.72 mmol) and NaOH (6.75 g, 135.44 mmol) was dissolved in THF (150 mL) and a small amount of water (50 mL). The solution was stirred for 1 h at 50 °C. The reaction was confirmed by TLC. The pH of the solution was adjusted to 2 by careful addition of HCl (37%, w/w). After extracting with ethyl acetate, an organic layer was collected and washed with brine and dried over Na_2SO_4 .

After removing the solvent, the product was collected as a white solid. Yield: 23.5 g (93%). ^1H NMR (400 MHz, CDCl_3) δ 7.39 (m, *J* = 22.2, 13.5, 7.0 Hz, 5H), 7.13 (d, *J* = 7.5 Hz, 2H), 6.94 (d, *J* = 8.0 Hz, 2H), 5.09 (s, 2H), 4.59 (d, *J* = 6.5 Hz, 1H), 3.11 (ddd, *J* = 43.3, 13.8, 5.7 Hz, 2H), 1.40 (s, 9H). ^{13}C NMR (100 MHz, CDCl_3) δ 176.18, 157.93, 155.45, 137.02, 130.48, 128.59, 127.97, 127.50, 114.95, 80.20, 70.01, 60.55, 37.00, 28.32. (*m/z*) for $\text{C}_{21}\text{H}_{25}\text{NO}_5$: calcd, 394.16 [M + Na]⁺, 370.16 [M – H][–]; found, 394.1 [M + Na]⁺; 370.2 [M – H][–].

2-Amino-3-(4-benzyloxy-phenyl)-propionamide (3). (i) Compound 2 (12 g, 32.31 mmol) and *N,N*-diisopropylethylamine (8.35 g, 64.62 mmol) were dissolved in THF. Isobutyl chloroformate (4.85 g, 35.54 mmol) was slowly added and stirred for 1 h at room temperature. The reaction was confirmed by TLC. Then, ammonia was injected for 10 min and stirred overnight at room temperature. The reaction was confirmed by TLC. After the solvent was removed by rotary evaporation, washed with water, and extracted with ethyl acetate, an organic layer was collected, which then was washed with brine and dried over Na_2SO_4 . After drying, the crude compound was recrystallized with ethanol, and the pure product was collected as a white solid. Yield: 10.0 g (84%). ^1H NMR (400 MHz, CDCl_3) δ 7.57–7.31 (m, 5H), 7.18 (d, *J* = 7.9 Hz, 2H), 6.95 (d, *J* = 8.0 Hz, 2H), 5.73 (s, 1H), 5.31 (s, 1H), 5.06 (s, 2H), 4.33 (s, 1H), 3.04 (dd, *J* = 17.7, 6.8 Hz, 2H), 1.44 (s, 9H). ^{13}C NMR (100 MHz, CDCl_3) δ 174.11, 174.11, 157.88, 157.88, 157.59, 147.27, 136.95, 130.40, 130.40, 128.60, 128.60, 128.00, 128.00, 127.49, 127.49, 115.06, 115.06, 77.25, 69.99, 55.36, 37.56, 28.21. (*m/z*) for $\text{C}_{21}\text{H}_{26}\text{N}_2\text{O}_4$: calcd, 393.18 [M + Na]⁺; found, 393.2 [M + Na]⁺.

(ii) [2-(4-Benzyloxy-phenyl)-1-carbamoyl-ethyl]-carbamic acid *tert*-butyl ester (20 g, 53.99 mmol) was dissolved in dichloromethane (200 mL), and trifluoroacetic acid (20 mL) was carefully added and stirred for 12 h at room temperature. The reaction was confirmed by TLC. The solvent was removed and a small amount of ethyl acetate was added to dissolve the crude product, and then sedimentation with hexane was performed. After precipitation, the substance was dried and collected as a white solid. Yield: 10.0 g (66%). ^1H NMR (400 MHz, DMSO) δ 7.39 (m, 5H), 7.17 (d, *J* = 8.0 Hz, 2H), 6.99 (d, *J* = 8.1 Hz, 2H), 5.08 (s, 2H), 3.87 (t, *J* = 6.4 Hz, 1H), 2.95 (dddd, *J* = 21.7, 14.0, 6.7 Hz, 2H). ^{13}C NMR (100 MHz, CDCl_3) δ 170.28, 158.00, 137.54, 131.06, 128.92, 128.34, 128.17, 127.46, 115.24, 69.58; 54.01; 36.46. (*m/z*) for $\text{C}_{16}\text{H}_{18}\text{N}_2\text{O}_2$: calcd, 371.15 [M + H]⁺; found, 371.1 [M + H]⁺.

3-(4-Benzyloxy-phenyl)-propane-1,2-diamine (4). Compound 3 (10 g, 36.99 mmol) was dissolved in THF, followed by the addition of the boron hydrogen reagent (222 mL, 222 mmol); then the mixture was heated to reflux and reacted for 24 h. The reaction was confirmed by TLC. Twenty milliliters of methanol was added slowly under an ice bath, and then the mixture was heated to reflux for 30 min. After the solvent was removed, the pH of the solution was adjusted to 2 by careful addition of concentrated hydrochloric acid. Then, after washing with ethyl ether and extracting with water, a water layer was collected and NaOH was added to adjust the pH to 8–9. After extracting with DCM, an organic layer was collected, washed with brine, and dried over Na_2SO_4 . After drying, the pure product was collected as a white solid. Yield: 6.0 g (63%). ^1H NMR (400 MHz, CDCl_3) δ 7.59–7.28 (m, 5H), 7.11 (d, 2H), 6.94 (d, 2H), 5.04 (s, 2H), 2.92 (s, 1H), 2.87–2.61 (m, 2H), 2.49 (dd, *J* = 22.2, 10.4 Hz, 2H). ^{13}C NMR (100 MHz, DMSO) δ 157.37, 137.03, 131.41, 130.29, 128.62, 128.01, 127.53, 114.88, 70.01, 55.13, 47.97, 41.34. (*m/z*) for $\text{C}_{16}\text{H}_{20}\text{N}_2\text{O}$: calcd, 257.17 [M + H]⁺; found, 257.2 [M + H]⁺.

*{[3-(4-Benzyloxy-phenyl)-2-(bis-tert-butoxycarbonylmethyl-amino)-propyl]-tert-butoxycarbonylmethyl-amino}-acetic Acid *tert*-Butyl Ester (5)*. Compound 4 (5 g, 19.5 mmol), *N,N*-diisopropylethylamine (15.13 g, 117.03 mmol) and KI (0.32 g, 1.95 mmol) were dissolved in ACN (60 mL). Then, *tert*-butyl bromoacetate (22.82 g, 117.03 mmol) was added and stirred for 4 h in an 60 °C oil bath. The reaction was confirmed by TLC. Inorganic salts were filtered using a filter, and after the filtrate was washed with water and extracted with ethyl acetate, an organic layer was collected, washed with brine, and dried over Na_2SO_4 . After evaporation, the crude product was collected and purified by column chromatography

(silica, hexanes/EtOAc, 6:1). Yield: 9.0 g (65%). ^1H NMR (400 MHz, CDCl_3) δ 7.58–7.31 (m, 5H), 7.16 (d, $J = 8.1$ Hz, 2H), 6.88 (d, $J = 8.1$ Hz, 2H), 5.03 (s, 2H), 3.49 (d, $J = 25.3$ Hz, 8H), 3.10 (t, $J = 5.5$ Hz, 1H), 2.89 (m, 2H), 2.60 (m, 2H), 1.55–1.42 (d, 36H). ^{13}C NMR (100 MHz, CDCl_3) δ 171.44, 170.98, 157.01, 137.22, 132.69, 130.22, 128.58, 127.92, 127.53, 114.58, 77.25, 69.99, 56.25, 55.75, 54.98, 53.55, 35.94, 28.15. (m/z) for $\text{C}_{40}\text{H}_{60}\text{N}_2\text{O}_9$: calcd, 713.44 [$\text{M} + \text{H}$] $^+$; 735.42 [$\text{M} + \text{Na}$] $^+$; found, 713.5 [$\text{M} + \text{H}$] $^+$; 735.6 [$\text{M} + \text{Na}$] $^+$.

[[3-(4-Benzyloxy-phenyl)-2-(bis-carboxymethyl-amino)-propyl]-carboxymethyl-amino]-acetic Acid (6). Compound 5 (5 g, 7.02 mmol) was dissolved in dichloromethane (80 mL), and trifluoroacetic acid (16 mL) was carefully added and stirred for 12 h at room temperature. The reaction was confirmed by ^1H NMR. The solvent was removed and an appropriate amount of methanol was added. The solvent was swirl dried and repeated three times. After drying, the pure product was collected as a primrose yellow solid. Yield: 3.0 g (87%). ^1H NMR (400 MHz, D_2O) δ 7.54–7.22 (m, 5H), 7.08 (d, $J = 7.8$ Hz, 2H), 6.98–6.85 (d, 2H), 5.05 (s, 2H), 3.28–2.77 (m, 8H), 2.74–2.50 (m, 3H), 2.37 (t, $J = 12.6$ Hz, 1H), 2.11 (t, $J = 12.2$ Hz, 2H). ^{13}C NMR (100 MHz, D_2O) δ 172.91, 170.91, 170.29, 169.89, 157.06, 136.68, 130.05, 129.82, 128.04, 115.18, 114.75, 69.51, 60.5, 57.01, 56.04, 48.71. (m/z) for $\text{C}_{24}\text{H}_{28}\text{N}_2\text{O}_9$: 489.19 [$\text{M} + \text{H}$] $^+$; 487.17 [$\text{M} - \text{H}$] $^-$; found, 489.2 [$\text{M} + \text{H}$] $^+$; 487.2 [$\text{M} - \text{H}$] $^-$.

Mn-BnO-TyrEDTA. The ligand (compound 6) (0.620 g, 1.19 mmol) was dissolved in ultrapure water, and the pH of the solution was adjusted to 7.4 by careful addition of NaOH (1.0 M). Based on the NMR titration results, $\text{MnCl}_2 \cdot 4\text{H}_2\text{O}$ (0.217 g, 1.10 mmol) was slowly added and the resulting solution was stirred. Finally, the pH of the solution was readjusted to 7.4. After lyophilization, the product was collected as a solid. ESI-MS (m/z) for $\text{C}_{24}\text{H}_{24}\text{MnN}_2\text{O}_9$: calcd, 608.6 [$\text{M} + 3\text{Na}$] $^+$; 562.08 [$\text{M} + \text{Na}$] $^+$; found, 608.1 [$\text{M} + 3\text{Na}$] $^+$; 562.18 [$\text{M} + \text{Na}$] $^-$.

Relaxivity. Relaxivities were measured with a 0.5 T NMR contrast agent relaxation rate analyzer (PQ001, Shanghai Newmag Electronic Technology Co., Ltd.). Longitudinal (T_1) relaxation was acquired via an IR (inversion recovery) sequence using 10 inversion times of duration ranging between $0.05 \times T_1$ and $5 \times T_1$. For transverse (T_2) relaxation, the CPMG (Carr–Purcell–Meiboom–Gill) pulse sequence was used. The nonlinear least-squares fit of the average pixel was used to estimate T_1 and T_2 relaxation times. Then, r_1 and r_2 relaxivities were computed by the linear fit of T_1 and T_2 relaxation times for each concentration (pick five concentrations by half dilution, such as 0.03125, 0.0625, 0.125, 0.25, and 0.5 mM).

Estimates of 1-Octanol: the Water Partition Coefficient (Estimated log P). Log P values were estimated using high-performance liquid chromatography (HPLC 1640, Agilent) as follows: a Kromasil C4 column (150 mm \times 4.6 mm 100 Å); eluent A, ultrapure water; eluent B, 100% MeCN; gradient, 5% B from 0 to 1 min, 5–50% B from 1 to 10 min, 50–95% B from 10 to 11 min, 95% B from 11 to 12 min, 95 to 5% B from 12 to 13 min, and 5% B from 13 to 15 min; and flow rate at 0.7 mL/min (eluent ultrasonography 1 h in advance). A linear calibration curve correlating log P of four standards (DMSO, nitrobenzene, phenol, and pyridine) to HPLC retention time (t_R) under the above method conditions was generated. The estimated log P values of complexes Mn-EDTA and Mn-BnO-TyrEDTA were estimated from their corresponding t_R using this calibration curve.

Cytotoxicity Assay. Mn-BnO-TyrEDTA and Gd-EOB-DTPA (Primovist) were tested for cytotoxicity on mouse macrophages (RAW 264.7) cells. RAW 264.7 cells were provided by the Chinese Academy of Sciences Cell Bank (Shanghai, China). The cells were cultured in Dulbecco's modified Eagle's medium (DMEM)/high glucose (4.5 g/L glucose) containing 10% (v/v) fetal bovine serum (Biological Industries, Israel) and 1% (v/v) penicillin–streptomycin (Hyclone, Logan, UT) at 37 °C, 5% CO_2 , and saturated humidity. RAW 264.7 cells were plated in 96-well plates at 1×10^4 cells/well in 100 μL of complete media. Following incubation for 24 h, the cells were added with varying concentrations (31.25, 62.5, 125, 250, and 500 μM) of contrast agents. Each well was added with a 10 μL Cell Counting Kit-8 (CCK-8) solution (Boster Biological Technology,

Wuhan, China) and then incubated at 37 °C for 1 h; the absorbance of the samples was measured at 450 nm using a microplate reader (Thermo Scientific). Cell viability was calculated according to the manufacturer's protocol.

MR Image. Swiss mice (20 ± 5 g; Laboratory Animal Center of NSMC, Sichuan, China) were imaged with a 3.0 T MR scanner (Discovery MR750, GE Medical System, Milwaukee, WI) with a custom-made mice coil. Anesthesia was maintained by inhaling isoflurane (RWD Life Science, Shenzhen, China) through a face mask (Anesthetic Conc.: 0.8–1.5%; 20–30 mL O_2/kg). After baseline imaging, contrast agents (0.1 mmol/kg Mn or Gd) were administered, separately, and imaging was repeated in a dynamic fashion. Bromosulphthalein (BSP) as a competitive inhibitor was injected 30, 20, and 15 min before the injection of Mn. The mouse was imaged immediately after the injection of the contrast agents using gradient recalled echo T1-weighted imaging sequences for 20 min. MR images were obtained in the coronal plane, and MRI imaging parameters were TE = 2.7 ms, TR = 9.5 ms, FA = 30°, FOV = 80 mm \times 64 mm, matrix size = 320 \times 192, 44 slices, slice thickness = 1.0 mm, NEX = 1.0, and bandwidth = 62.50 kHz. Images were analyzed using a RadiAnt DICOM viewer by drawing regions of interest (ROIs) on the liver and kidneys. The normalized signal-to-noise ratio (nSNR) was used with $\text{nSNR} = \text{SNR}_{\text{post}}/\text{SNR}_{\text{pre}}$ and $\text{SNR} = \text{SI}/\text{SD}_{\text{air}}$, where SI is the signal intensity and SD_{air} is the standard deviation of the signal intensity in the ROI outside the animal. The contrast-to-noise ratio (CNR) values were calculated as $\text{CNR} = (\text{SI}_{\text{liver}} - \text{SI}_{\text{muscle}})/\text{SD}_{\text{air}}$, and ΔCNR values were calculated by subtracting the preinjection CNR map from the CNR map after contrast agent administration.

Real-Time Quantitative PCR Analysis and Immunofluorescence Staining. Human embryonic kidney (HEK-293) cells were provided by the Chinese Academy of Sciences Cell Bank (Shanghai, China). Human embryonic kidney cells stably overexpressing OATP1B1 (HEK-OATP1B1) were purchased from Genechem Co., Ltd (Shanghai, China). The cells were tested for the OATP1B1 receptor by real-time fluorescent quantitative PCR and immunofluorescence. The RNA was extracted from HEK-293 cells and HEK-OATP1B1 cells using the TRIzol method, and the mRNA expression levels of OATP1B1 were detected by SYBR green gene expression assays (primer OATP1B1: forward primer, 5'-AACTCCTACT-GATTCTCGATGGG-3' and reverse primer, 5'-GTTTCCAGCA-CATGCAAAGAC-3'. Primer GAPDH: forward primer, 5'-TGACTTCAACAGCGACACC-CA-3' and reverse primer, 5'-CACCTGTTGCTGTAGCCA-AA-3'). Immunofluorescence images were recorded using an Olympus laser scanning confocal microscope. The cells were fixed with PFA, permeabilized in 0.1% Triton X-100, and then blocked in 5% BSA for 1 h at 25 °C. The samples were incubated with the SLCO1B1 antibody (Affinity Biosciences) at 4 °C overnight. The expression of the transporter protein was assessed using the Alexa Fluor 594 conjugated goat anti-rabbit antibody (Affinity Biosciences).

Cell Uptake Assay. HEK-OATP1B1 cells and HEK-293 cells were seeded in 12-well plates at 10 000 cells per well. After 24 h of incubation, the cells were incubated with 0.1 mM Mn-BnO-TyrEDTA at 37 °C for 0, 5, 10, 20, and 30 min, washed with ice-cold phosphate-buffered saline, and then disintegrated using 1% HNO_3 . In inhibition assays, the uptake of Mn-BnO-TyrEDTA (0.1 mM) was measured at 10 min in the absence (control) and presence of 0.1 mM BSP. Prewarmed (37 °C) uptake buffer (142 mM NaCl, 5 mM KCl, 1 mM K_2HPO_4 , 1.2 mM MgSO_4 , 1.5 mM CaCl_2 , 5 mM glucose, and 12.5 mM HEPES, pH 7.3–7.4) was used as a cell culture medium.⁴¹ The concentration of Mn was quantified in cell lysates by inductively coupled plasma mass spectrometry (ICP-MS), and the protein concentration of each sample was determined using the BCA protein concentration determination kit (Boster Biological Technology, Wuhan, China). The Michaelis–Menten constant (K_m) and the maximum transport velocity (V_{max}) were calculated using the following equation: $y = V_{\text{max}} \times x/(K_m + x)$.¹²

Biodistribution and Biliary Excretion Studies. Swiss mice were used in the biodistribution study. After intravenous injection of Mn-BnO-TyrEDTA (0.1 mmol/kg) to normal male and female mice

($n = 6$; 20 ± 5 g) through tail veins, the mice were euthanized postinjection at 4 different time points (5 min, 30 min, 1 h, and 24 h). Various tissues (brain, heart, liver, spleen, lung, kidneys, bone, muscle, and small intestine) were weighed and then digested in concentrated nitric acid for 48 h. Samples for analysis were prepared by diluting them in an aqueous solution of 0.1% Triton X and 5% HNO₃. The manganese concentration of the sample was quantitatively analyzed by ICP-MS. The total amount of bile excretion was calculated based on the test results. An arterial cannula (i.d., 0.6 mm; Linhua, Suzhou, China) was introduced into the ductus choledochal of six SD rats (180–220 g) while the animals were kept under anesthesia. Rats were anesthetized with isoflurane and administered 0.1 mmol/kg Mn-BnO-TyrEDTA injection into the tail vein. Bile was collected quantitatively before and 5, 10, 15, 20, 30, 40, 50, 60, 70, and 80 min after contrast medium administration. The concentration of the contrast medium in the bile was determined by measuring [Mn] using ICP-MS.

Pharmacokinetic Study. Sprague-Dawley (SD) rats (200 ± 20 g; Laboratory Animal Center of North Sichuan Medical College (NSMC), Sichuan, China) were used in the pharmacokinetic study. The rats ($n = 6$) were anesthetized by isoflurane (Anesthetic Conc.: 2–2.5%; 25–35 mL O₂/kg). The tail vein cannula was used for administration at a dose of 0.1 mmol/kg, and the carotid artery catheter was used for blood sampling. Approximately 100 μ L of blood was collected at 0 (predose to serve as a blank), 0.33, 0.67, 1, 1.5, 2, 2.5, 3, 4, 5, 7, 10, 15, 20, 25, and 30 min postdose from the carotid artery via a catheter after IV administration of Mn-BnO-TyrEDTA. The samples were diluted with 0.1% Triton X-100 (Inno-chem Science & Technology, Beijing, China) in 5% nitric acid.²⁷ Manganese samples were quantified by elemental analysis by ICP-MS.⁴² Quantitative analysis was performed using a linear calibration curve ranging from 0.1 to 200 ppb Mn calibration standard manufactured under ISO 9001 quality assurance system by PerkinElmer. The blood pharmacokinetic data were fit to the following biexponential model $C(t) = A \exp(-\alpha t) + B \exp(-\beta t)$, where $C(t)$ is the manganese metal ion concentration at time t , α and β are the distribution and elimination rates, respectively, and A and B are the distribution and elimination coefficients, respectively.²⁵ A two-compartment pharmacokinetic model was used to analyze the data and calculate the pharmacokinetic parameters with PKSolver software (China Pharmaceutical University).⁴³ The compartment model fitting evaluation standard is based on the akaike information criterion (AIC) and R-squared (R^2).

Data Analysis. Data analysis was performed using Graphpad Prism 8 software. Statistical analysis was performed using unpaired Student's t -test. P values less than 0.05 were considered to indicate statistical significance.

■ ASSOCIATED CONTENT

SI Supporting Information

The Supporting Information is available free of charge at <https://pubs.acs.org/doi/10.1021/acs.jmedchem.1c00393>.

ESI-MS and NMR spectrum (¹H and ¹³C NMR spectra) of compounds 2–6 and Mn-BnO-TyrEDTA; HPLC trace of Mn-BnO-TyrEDTA; NMR titration for determining the precise Mn/L ratio; HPLC trace for determining the estimated Log P ; and liquid chromatography-mass spectrometry (LC-MS) traces analysis of urine and feces (PDF)

Compounds 1–6 and Mn-BnO-TyrEDTA as molecular formula strings (CSV)

■ AUTHOR INFORMATION

Corresponding Authors

Xiaoming Zhang – Sichuan Key Laboratory of Medical Imaging, North Sichuan Medical College, Nanchong 637000, China; Department of Radiology, Affiliated Hospital of North Sichuan Medical College, Nanchong 637000, China;

Phone: (+)86-817-2242635; Email: zhangxm@nsmc.edu.cn

Jiang Zhu – Sichuan Key Laboratory of Medical Imaging, School of Pharmacy, and Nanchong Key laboratory of MRI Contrast Agent, North Sichuan Medical College, Nanchong 637000, China; Department of Oncology, Affiliated Hospital of North Sichuan Medical College, Nanchong 637000, China; orcid.org/0000-0001-7437-2956; Phone: (+)86-181-81085956; Email: zhujiang@nsmc.edu.cn

Authors

Keyu Chen – Sichuan Key Laboratory of Medical Imaging and School of Pharmacy, North Sichuan Medical College, Nanchong 637000, China

Pan Li – Department of Radiotherapy, Sichuan Cancer Hospital & Institute, Chengdu 610041, China

Chunrong Zhu – Sichuan Key Laboratory of Medical Imaging and College of Preclinical Medicine, North Sichuan Medical College, Nanchong 637000, China

Zhiyang Xia – Sichuan Key Laboratory of Medical Imaging and College of Preclinical Medicine, North Sichuan Medical College, Nanchong 637000, China

Qian Xia – Sichuan Key Laboratory of Medical Imaging and Nanchong Key laboratory of MRI Contrast Agent, North Sichuan Medical College, Nanchong 637000, China

Lei Zhong – Sichuan Key Laboratory of Medical Imaging and Nanchong Key laboratory of MRI Contrast Agent, North Sichuan Medical College, Nanchong 637000, China

Bin Xiao – Sichuan Key Laboratory of Medical Imaging, North Sichuan Medical College, Nanchong 637000, China

Tao Cheng – Sichuan Key Laboratory of Medical Imaging, North Sichuan Medical College, Nanchong 637000, China

Changqiang Wu – Sichuan Key Laboratory of Medical Imaging and Nanchong Key laboratory of MRI Contrast Agent, North Sichuan Medical College, Nanchong 637000, China; orcid.org/0000-0002-6363-2721

Chengyi Shen – College of Preclinical Medicine and Nanchong Key laboratory of MRI Contrast Agent, North Sichuan Medical College, Nanchong 637000, China

Complete contact information is available at: <https://pubs.acs.org/doi/10.1021/acs.jmedchem.1c00393>

Author Contributions

K.C. and P.L. contributed equally. The manuscript was written through contributions of all authors. All authors have given approval to the final version of the manuscript.

Notes

The authors declare no competing financial interest.

■ ACKNOWLEDGMENTS

The authors acknowledge financial support from the National Nature Science Foundation of China (81671675, 21172025, and 81601490) and Science and Technology Project of Municipal School Strategic Cooperation, Nanchong (NSMC20170100, 18SXHZ0091, 18SXHZ0379, and NCKL201704).

■ ABBREVIATIONS USED

BSP, bromosulfophthalein; DCE, dynamic contrast-enhanced; EDTA, ethylenediaminetetraacetic acid; GBCA, gadolinium-based MRI contrast agent; ICP-MS, inductively coupled plasma mass spectrometry; MRI, magnetic resonance imaging;

OATPs, organic anion transporting peptides; SPGR-T1WI, spoiled gradient recalled echo T1-weighted images

REFERENCES

- (1) Rudin, M.; Weissleder, R. Molecular imaging in drug discovery and development. *Nat. Rev. Drug Discovery* **2003**, *2*, 123–131.
- (2) Bellin, M. F.; Vasile, M.; Morel-Precetti, S. Currently used non-specific extracellular MR contrast media. *Eur. Radiol.* **2003**, *13*, 2688–2698.
- (3) Allard, M.; Doucet, D.; Kien, P.; Bonnemain, B.; Caille, J. M. Experimental study of DOTA-gadolinium. Pharmacokinetics and pharmacologic properties. *Invest. Radiol.* **1988**, *23*, S271–274.
- (4) Tweedle, M. F.; Wedeking, P.; Kumar, K. Biodistribution of radiolabeled, formulated gadopentetate, gadoteridol, gadoterate, and gadodiamide in mice and rats. *Invest. Radiol.* **1995**, *30*, 372–380.
- (5) Chong, H. S.; Garmestani, K.; Bryant, L. H., Jr.; Milenic, D. E.; Overstreet, T.; Birch, N.; Le, T.; Brady, E. D.; Brechbiel, M. W. Synthesis and evaluation of novel macrocyclic and acyclic ligands as contrast enhancement agents for magnetic resonance imaging. *J. Med. Chem.* **2006**, *49*, 2055–2062.
- (6) Bellin, M. F.; Van Der Molen, A. J. Extracellular gadolinium-based contrast media: an overview. *Eur. J. Radiol.* **2008**, *66*, 160–167.
- (7) Aime, S.; Caravan, P. Biodistribution of gadolinium-based contrast agents, including gadolinium deposition. *J. Magn. Reson. Imaging* **2009**, *30*, 1259–1267.
- (8) Garcia, J.; Liu, S. Z.; Louie, A. Y. Biological effects of MRI contrast agents: gadolinium retention, potential mechanisms and a role for phosphorus. *Philos. Trans. R. Soc., A* **2017**, *375*, No. 20170180.
- (9) Van Beers, B. E.; Pastor, C. M.; Hussain, H. K. Primovist, Eovist: what to expect? *J. Hepatol.* **2012**, *57*, 421–429.
- (10) Grazioli, L.; Bondioni, M. P.; Haradome, H.; Motosugi, U.; Tinti, R.; Frittoli, B.; Gambarini, S.; Donato, F.; Colagrande, S. Hepatocellular adenoma and focal nodular hyperplasia: value of gadoxetic acid-enhanced MR imaging in differential diagnosis. *Radiology* **2012**, *262*, S20–S29.
- (11) McInnes, M. D.; Hibbert, R. M.; Inacio, J. R.; Schieda, N. Focal Nodular Hyperplasia and Hepatocellular Adenoma: Accuracy of Gadaxetic Acid-enhanced MR Imaging-A Systematic Review. *Radiology* **2015**, *277*, 927.
- (12) Leonhardt, M.; Keiser, M.; Oswald, S.; Kuhn, J.; Jia, J.; Grube, M.; Kroemer, H. K.; Siegmund, W.; Weitschies, W. Hepatic uptake of the magnetic resonance imaging contrast agent Gd-EOB-DTPA: role of human organic anion transporters. *Drug Metab. Dispos.* **2010**, *38*, 1024–1028.
- (13) Tsuboyama, T.; Onishi, H.; Kim, T.; Akita, H.; Hori, M.; Tsumi, M.; Nakamoto, A.; Nagano, H.; Matsuura, N.; Wakasa, K.; Tomoda, K. Hepatocellular carcinoma: hepatocyte-selective enhancement at gadoxetic acid-enhanced MR imaging—correlation with expression of sinusoidal and canalicular transporters and bile accumulation. *Radiology* **2010**, *255*, 824–833.
- (14) Nassif, A.; Jia, J.; Keiser, M.; Oswald, S.; Modess, C.; Nagel, S.; Weitschies, W.; Hosten, N.; Siegmund, W.; Kuhn, J. P. Visualization of hepatic uptake transporter function in healthy subjects by using gadoxetic acid-enhanced MR imaging. *Radiology* **2012**, *264*, 741–750.
- (15) Ueno, A.; Masugi, Y.; Yamazaki, K.; Komuta, M.; Effendi, K.; Tanami, Y.; Tsujikawa, H.; Tanimoto, A.; Okuda, S.; Itano, O.; Kitagawa, Y.; Kuribayashi, S.; Sakamoto, M. OATP1B3 expression is strongly associated with Wnt/beta-catenin signalling and represents the transporter of gadoxetic acid in hepatocellular carcinoma. *J. Hepatol.* **2014**, *61*, 1080–1087.
- (16) Lu, C. C.; Chen, W. K.; Chiang, J. H.; Tsai, Y. F.; Juan, Y. N.; Lin, P. C.; Tyan, Y. S.; Yang, J. S. cDNA Microarray Analysis and Influx Transporter OATP1B1 in Liver Cells After Exposure to Gadaxetic Disodium, a Gadolinium-based Contrast Agent in MRI Liver Imaging. *In Vivo* **2018**, *32*, 677–684.
- (17) Sadowski, E. A.; Bennett, L. K.; Chan, M. R.; Wentland, A. L.; Garrett, A. L.; Garrett, R. W.; Djamali, A. Nephrogenic systemic fibrosis: risk factors and incidence estimation. *Radiology* **2007**, *243*, 148–157.
- (18) Juluru, K.; Vogel-Claussen, J.; Macura, K. J.; Kamel, I. R.; Steever, A.; Bluemke, D. A. MR imaging in patients at risk for developing nephrogenic systemic fibrosis: protocols, practices, and imaging techniques to maximize patient safety. *Radiographics* **2009**, *29*, 9–22.
- (19) Weinreb, J. C.; Abu-Alfa, A. K. Gadolinium-based contrast agents and nephrogenic systemic fibrosis: why did it happen and what have we learned? *J. Magn. Reson. Imaging* **2009**, *30*, 1236–1239.
- (20) Idée, J. M.; Fretellier, N.; Robic, C.; Corot, C. The role of gadolinium chelates in the mechanism of nephrogenic systemic fibrosis: A critical update. *Crit. Rev. Toxicol.* **2014**, *44*, 895–913.
- (21) Ramalho, J.; Semelka, R. C.; Ramalho, M.; Nunes, R. H.; AIObaidy, M.; Castillo, M. Gadolinium-Based Contrast Agent Accumulation and Toxicity: An Update. *Am. J. Neuroradiology* **2016**, *37*, 1192–1198.
- (22) Fraum, T. J.; Ludwig, D. R.; Bashir, M. R.; Fowler, K. J. Gadolinium-based contrast agents: A comprehensive risk assessment. *J. Magn. Reson. Imaging* **2017**, *46*, 338–353.
- (23) Pasquini, L.; Napolitano, A.; Visconti, E.; Longo, D.; Romano, A.; Toma, P.; Rossi Espagnet, M. C. Gadolinium-Based Contrast Agent-Related Toxicities. *CNS Drugs* **2018**, *32*, 229–240.
- (24) Schieda, N.; Blaichman, J. I.; Costa, A. F.; Glikstein, R.; Hurrell, C.; James, M.; Jabehdar Maralani, P.; Shabana, W.; Tang, A.; Tsampalieros, A.; van der Pol, C.; Hiremath, S. Gadolinium-Based Contrast Agents in Kidney Disease: Comprehensive Review and Clinical Practice Guideline Issued by the Canadian Association of Radiologists. *Can. Assoc. Radiol., J.* **2018**, *69*, 136–150.
- (25) Gale, E. M.; Wey, H. Y.; Ramsay, I.; Yen, Y. F.; Sosnovik, D. E.; Caravan, P. A Manganese-based Alternative to Gadolinium: Contrast-enhanced MR Angiography, Excretion, Pharmacokinetics, and Metabolism. *Radiology* **2018**, *286*, 865–872.
- (26) Ndiaye, D.; Sy, M.; Pallier, A.; Meme, S.; de Silva, I.; Lacerda, S.; Nonat, A. M.; Charbonniere, L. J.; Toth, E. Unprecedented Kinetic Inertness for a Mn(2+) -Bispidine Chelate: A Novel Structural Entry for Mn(2+) -Based Imaging Agents. *Angew. Chem., Int. Ed.* **2020**, *59*, 11958–11963.
- (27) Wang, J.; Wang, H.; Ramsay, I. A.; Erstad, D. J.; Fuchs, B. C.; Tanabe, K. K.; Caravan, P.; Gale, E. M. Manganese-Based Contrast Agents for Magnetic Resonance Imaging of Liver Tumors: Structure–Activity Relationships and Lead Candidate Evaluation. *J. Med. Chem.* **2018**, *61*, 8811–8824.
- (28) Aime, S.; Anelli, L.; Botta, M.; Brocchetta, M.; Canton, S.; Fedeli, F.; Gianolio, E.; Terreno, E. Relaxometric evaluation of novel manganese(II) complexes for application as contrast agents in magnetic resonance imaging. *JBIC, J. Biol. Inorg. Chem.* **2002**, *7*, 58–67.
- (29) Troughton, J. S.; Greenfield, M. T.; Greenwood, J. M.; Dumas, S.; Wiethoff, A. J.; Wang, J.; Spiller, M.; McMurry, T. J.; Caravan, P. Synthesis and evaluation of a high relaxivity manganese(II)-based MRI contrast agent. *Inorg. Chem.* **2004**, *43*, 6313–6323.
- (30) Vanasschen, C.; Molnar, E.; Tircso, G.; Kalman, F. K.; Toth, E.; Brandt, M.; Coenen, H. H.; Neumaier, B. Novel CDTA-based, Bifunctional Chelators for Stable and Inert Mn(II) Complexation: Synthesis and Physicochemical Characterization. *Inorg. Chem.* **2017**, *56*, 7746–7760.
- (31) Zhu, J.; Gale, E. M.; Atanasova, I.; Rietz, T. A.; Caravan, P. Hexameric Mn(II) dendrimer as MRI contrast agent. *Chem. - Eur. J.* **2014**, *20*, 14507–14513.
- (32) Tóth, É.; Helm, L.; Merbach, A. Relaxivity of Gadolinium(III) Complexes: Theory and Mechanism. In *The Chemistry of Contrast Agents in Medical Magnetic Resonance Imaging*; Merbach, A.; Helm, L.; Tóth, É., Eds.; John Wiley & Sons, Ltd: Chichester, UK, 2013; pp 2025–2081.
- (33) Greiser, J.; Weigand, W.; Freesmeyer, M. Metal-Based Complexes as Pharmaceuticals for Molecular Imaging of the Liver. *Pharmaceuticals* **2019**, *12*, No. 137.

(34) Schuhmann-Giampieri, G.; Schmitt-Willich, H.; Press, W. R.; Negishi, C.; Weinmann, H. J.; Speck, U. Preclinical evaluation of Gd-EOB-DTPA as a contrast agent in MR imaging of the hepatobiliary system. *Radiology* **1992**, *183*, 59–64.

(35) Reimer, P.; Schneider, G.; Schima, W. Hepatobiliary contrast agents for contrast-enhanced MRI of the liver: properties, clinical development and applications. *Eur. Radiol.* **2004**, *14*, 559–578.

(36) Schuhmann-Giampieri, G. Liver contrast media for magnetic resonance imaging Interrelations between pharmacokinetics and imaging. *Invest. Radiol.* **1993**, *28*, 753–761.

(37) Karlgren, M.; Vildhede, A.; Norinder, U.; Wisniewski, J. R.; Kimoto, E.; Lai, Y.; Haglund, U.; Artursson, P. Classification of Inhibitors of Hepatic Organic Anion Transporting Polypeptides (OATPs): Influence of Protein Expression on Drug–Drug Interactions. *J. Med. Chem.* **2012**, *55*, 4740–4763.

(38) Clément, O.; Muhler, A.; Vexler, V.; Berthezene, Y.; Brasch, R. C. Gadolinium-ethoxybenzyl-DTPA, a new liver-specific magnetic resonance contrast agent. Kinetic and enhancement patterns in normal and cholestatic rats. *Invest. Radiol.* **1992**, *27*, 612–619.

(39) van Montfoort, J. E.; Stieger, B.; Meijer, D. K.; Weinmann, H. J.; Meier, P. J.; Fattinger, K. E. Hepatic uptake of the magnetic resonance imaging contrast agent gadoxetate by the organic anion transporting polypeptide Oatp1. *J. Pharmacol. Exp. Ther.* **1999**, *290*, 153–157.

(40) Obaidat, A.; Roth, M.; Hagenbuch, B. The expression and function of organic anion transporting polypeptides in normal tissues and in cancer. *Annu. Rev. Pharmacol. Toxicol.* **2012**, *52*, 135–151.

(41) Seithel, A.; Eberl, S.; Singer, K.; Auge, D.; Heinkele, G.; Wolf, N. B.; Dorje, F.; Fromm, M. F.; König, J. The influence of macrolide antibiotics on the uptake of organic anions and drugs mediated by OATP1B1 and OATP1B3. *Drug Metab. Dispos.* **2007**, *35*, 779–786.

(42) Erstad, D. J.; Ramsay, I. A.; Jordan, V. C.; Sojoodi, M.; Fuchs, B. C.; Tanabe, K. K.; Caravan, P.; Gale, E. M. Tumor Contrast Enhancement and Whole-Body Elimination of the Manganese-Based Magnetic Resonance Imaging Contrast Agent Mn-PyC3A. *Invest. Radiol.* **2019**, *54*, 697–703.

(43) Zhang, Y.; Huo, M.; Zhou, J.; Xie, S. PKSolver: An add-in program for pharmacokinetic and pharmacodynamic data analysis in Microsoft Excel. *Comput. Methods Programs Biomed.* **2010**, *99*, 306–314.